FULL PAPER

Reactive Aramid Nanostructures as High-Performance Polymeric Building Blocks for Advanced Composites

*Keqin Cao, Carlos Pons Siepermann, Ming Yang, Anthony M. Waas, Nicholas A. Kotov, M. D. Thouless, and Ellen M. Arruda**

Traditionally, the field of advanced nanocomposites has relied on a fairly limited set of building blocks; many with low reactivity and of limited variability. These limitations have been addressed by the creation of functionalized nanometer-scale aramid structures, in the form of nanofibers and nanosheets. These were obtained by deprotonating macroscale, commercial Kevlar yarns using potassium hydroxide in dimethyl sulfoxide to yield stable dispersions of nanometer-scale aramid fibers that were then hydrolyzed using phosphoric acid (PA). To illustrate the use of these functionally-active nanostructures as building blocks for nanocomposites, they were crosslinked by glutaraldehyde (GA), and formed into macroscopic thin films by vacuum-assisted filtration. It was shown that the mechanical properties of these PA/GA treated films can be tuned by varying the amounts of PA and GA used during synthesis, adjusting the relative amounts of hydrolysis and polymerization. These results are the first demonstration that aramid nanometer-scale fibers can be used to form versatile nanometer-sized building blocks that can then be crosslinked to fabricate a wide variety of nanostructured aramid materials with tailorable properties.

1. Introduction

Much of the recent work on nanocomposite mechanics focuses on improving attributes of the reinforcement phase (e.g., dispersion).[1–4] However, the design of high-performance nanocomposites also requires polymeric matrices with superior mechanical properties and versatile techniques to tailor these matrices. Suitable polymeric nanometer-scale building blocks for advanced composite matrices can be prepared from conventionally strong materials. Poly-paraphenylene terephthalamide (PPTA), a high performance para-aramid polymer better known by its trade-name Kevlar, has exceptional stiffness and strength, and serves as a promising candidate for such a matrix material. A Kevlar microfiber is anisotropic and its stiff and highly-aligned backbone results in a modulus of 85 GPa and a tensile strength of 3.9 GPa along the fiber axis (**Figure 1**a).[5] Relying on such superior mechanical properties, aramid microfibers have been used to reinforce high-ductility, low-stiffness polymers, to raise the stiffness and yield strength of polymer matrix composites while preserving toughness.[6–8] However, this approach using Kevlar microfibers has been hindered by the lack of an effective way to promote or improve the adhesion between aramid fibers and polymer matrices. The same problem of weak adhesion between aramid fibers and inorganic nanometer-scale components such as carbon nanotubes has also limited their use in nanocomposites.[9]

The paradigm of aramid microfibers as relatively inert and possessing a low affinity for surface bonding has long been recognized. This has motivated many efforts to develop techniques such as hydrolysis or surface coating to enhance the interaction between Kevlar and other materials.[6–8,10–14] The surface of an aramid microfiber contains a limited number of reactive sites to bond with other materials,[15,16] and the core is an inert region consisting of closely packed macromolecular chains with a high density of hydrogen bonds between them. The low surface to volume ratio of a microfiber results in chemically stable fibers (Figure 1c) and yarns (Figure 1d). To overcome this problem of scale, we took advantage of a method recently developed in our laboratory to make aramid nanofibers (ANFs) with diameters between 3 and 30 nm, and up to 10 μm in length (Figure 1b).[17] By substantially increasing the surface area to volume ratio, ANFs greatly increase the potential number of surface functional groups per unit volume that can be made available for interactions with other phases.

Previous research has reported that acid-catalyzed hydrolysis of aramid microfibers results in improved interfacial strength

K. Cao, Prof. A. M. Waas, Prof. M. D. Thouless, Prof. E. M. Arruda
Department of Mechanical Engineering
University of Michigan
Ann Arbor, MI 48109-2136, USA
E-mail: arruda@umich.edu
C. P. Siepermann, Dr. M. Yang, Prof. N. A. Kotov
Department of Chemical Engineering
University of Michigan
Ann Arbor, MI 48109-2136, USA
Prof. A. M. Waas
Department of Aerospace Engineering
University of Michigan
Ann Arbor, MI 48109-2136, USA
Prof. N. A. Kotov, Prof. M. D. Thouless
Department of Materials Science and Engineering
University of Michigan
Ann Arbor, MI 48109-2136, USA
Prof. N. A. Kotov, Prof. E. M. Arruda
Department of Biomedical Engineering
Program in Macromolecular Science and Engineering
University of Michigan
Ann Arbor, MI 48109-2136, USA

DOI: 10.1002/adfm.201202466

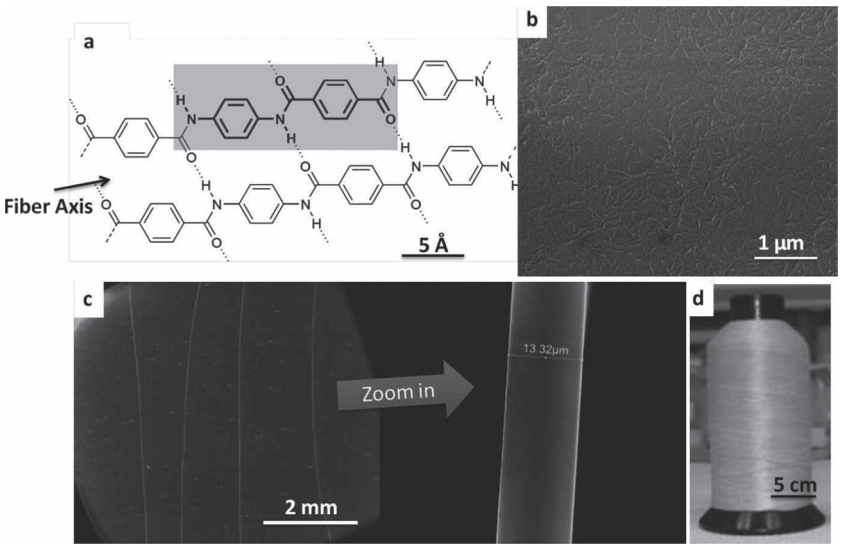

Figure 1. Aramids at various scales, from small to large. a) Chemical structure of aramid fiber. The monomer (bold) has an amide linkage bonded between two aromatic rings. The parallel molecular orientation of the crystalline fiber results in its anisotropy, with high stiffness and strength along the fiber axis. b) ANFs with diameters varying from 3 to 30 nm and lengths up to 10 μm, deposited on a substrate and observed in an SEM (see ref. [17] for further details). c) Aramid microfibers with diameters of around 14 μm separated from commercial Kevlar yarns (d) and observed in an SEM. d) Commercial Kevlar yarns used as fiber reinforcement or woven into mats.

between aramid microfibers and epoxy matrices owing to additional functional groups introduced on the microfiber surfaces.[11,12] Based on this result, we show that phosphoric acid (PA) catalyzed hydrolysis can be used to generate reactive NH_2 and COOH functional groups on ANFs for bonding with glutaraldehyde (GA). Interestingly, after the PA treatment, ANFs are converted into nanometer-scale building blocks with other morphologies, denoted here as aramid nanosheets, both of which can be assembled into nanostructured 60-mm diameter × 10–25-μm-thick films after GA polymerization by means of vacuum-assisted filtration. Various characterization methods are used to illustrate the effects of the extent of PA/GA treatments on the mechanical properties and morphologies of these aramid nanostructured films. The understanding that was developed by these studies of how to control the nanostructure, morphology and properties of the aramid nanostructured networks is expected to provide a basis for future work on the optimization of aramid-based structures for high-performance nanocomposites.

2. Results and Discussion

High surface-to-volume ratio aramid nanofibers (ANFs) obtained from macroscopic-scale fibers after deprotonation of amide groups[17] can form the basis of a new generation of nanostructured materials. Here, we demonstrate that the ANFs can be made chemically reactive with useful functional groups for bonding, and that these reactive aramid building blocks can be assembled into transversely isotropic networks with tailored nanostructures, morphologies and properties. Uniaxial tensile tests at room temperature and dynamic mechanical analyses (DMA) over a wide range of temperatures were used to characterize the mechanical properties of the aramid nanostructured networks. The reaction mechanisms during the phosphoric acid/ glutaraldehyde (PA/GA) treatment of the Kevlar and the resultant bonding and morphology of the networks were explored using (i) Fourier-transform infrared spectroscopy (FTIR) to probe the chemical structures, (ii) transmission electron microscopy (TEM) to visualize the morphologies, and (iii) thermogravimetric analysis (TGA) to characterize the thermal properties of the nanostructured networks.

2.1. Tuned Mechanical Properties of Aramid Nanostructured Networks

2.1.1. Synthesis

A family of aramid nanostructured films was prepared by reacting a Kevlar/potassium hydroxide (KOH)/dimethyl sulfoxide (DMSO) solution of ANFs with various amounts of PA and GA and PA/GA ratios. Also, an ANF network with no treatment was made as a comparison by adding water to the ANF solution (see the Experimental Section). After chemical treatment, films were fabricated from the solution by vacuum-assisted filtration to obtain continuous and homogeneous structures. The nine different conditions used to prepare this family are shown in **Figure 2**a, along with optical scopy images of several of the resultant products. The surface and the cross-section of the filtered films with and without treatment were also observed in SEM, as discussed in the Supporting Information. The surfaces of the films appeared smooth under 8000× magnification and at higher magnification, a densely packed structure was revealed. The cross section of the films showed a layered structure created by the filtration process. The thickness of the films was uniform with a small variation of ≈3%. It should be noted that it was not possible to form a continuous and homogeneous film with ANF solutions that had been exposed to PA but not to GA, or from solutions exposed to GA but not to PA, (Figure 2a "No PA" and "No GA" samples).

2.1.2. Unaixial Tensile Testing

The mechanical properties of the PA/GA treated films were tuned by varying the PA/GA ratio and the extent of the PA/GA treatment, as characterized by room-temperature uniaxial tensile testing at a strain rate of 0.005/s. Figure 2b illustrates how increased hydrolysis (more PA) tends to result in a more compliant material, while increased polymerization (more GA) tends to result in a stiffer material. A finite level of hydrolysis is required to provide active sites for the reaction with the GA, as the "No PA" sample does not form a continuous network. GA is not able to form bonds with the inert aramid unless water

a 100 mg of Kevlar in 100 mL DMSO	PA (mL)	GA (mL)	Thickness (μm)	Young's Modulus (GPa)	Yield Strength (MPa)	Strain Energy Density (MJ/m³)
No Treatment	0	0	13 ± 0.7	7.1 ± 0.3	53 ± 2	8.0 ± 0.1
Sample A	0.25	1.5	20 ± 1.0	8.5 ± 0.3	83 ± 3	6.7 ± 1.8
Sample B	1.0	1.5	10 ± 0.6	7.4 ± 0.3	65 ± 3	6.9 ± 0.5
Sample C	1.0	1.0	25 ± 1.4	4.5 ± 0.1	34 ± 2	7.3 ± 0.4
Sample D	2.5	3.5	10 ± 0.7	2.2 ± 0.4	25 ± 4	5.1 ± 0.6
Sample E	2.5	3.0	20 ± 1.1	1.5 ± 0.4	13 ± 3	2.9 ± 0.4
No PA	0	1.5	-	-	-	-
No GA	0.25	0	-	-	-	-
Sample A+	0.25	3.5	10 ± 0.8	8.0 ± 0.9	82 ± 9	8.3 ± 1.9

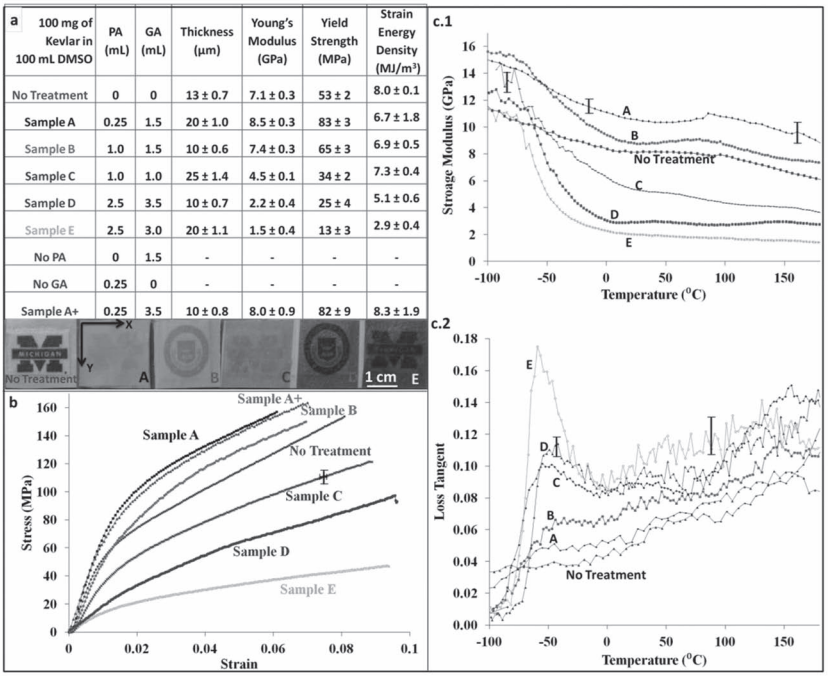

Figure 2. a) Aramid nanostructured networks assembled by vacuum-assisted filtration with varied PA and GA contents used in synthesis. ANF network with no treatment was made as a comparison. Continuous and homogenous networks were successfully obtained from each treatment, except for the samples made with just PA (No GA) or just GA (No PA). The isotropy of the samples was checked by testing specimens in the *X–Y* plane with different orientations. The thickness of the samples refers to the out-of-plane dimension. The differences in the apparent transparency among samples may come from differences in the film thickness. b) Stress-strain curves of aramid films as functions of PA and GA contents characterized by uniaxial tensile tests at a strain rate of 0.005/s at room temperature. The mechanical properties of these nanostructured networks were tuned by the extent of PA/GA treatment. Multiple tests were performed on each sample until fracture, and consistent results were obtained. c) Storage modulus and loss tangent as a function of temperature of the networks with and without PA/GA treatment at a frequency of 1Hz and a strain of 0.25 ± 0.10%. At a given temperature above about –70 °C, the storage modulus increased with a reduced amount of PA or with an increased amount of GA, as also indicated by the uniaxial tension tests. The transition indicated by the peak in the loss-tangent curves at around –70 °C dropped from Sample E to the "No Treatment" sample.

is used as in the "No Treatment" case, to re-protonate aramid macromolecules so that they form a film through hydrogen bonding. In particular, a limited amount of PA hydrolysis followed by reaction with GA (Samples A and B) produces networks that are stiffer than the untreated material. However, as can be seen by a comparison of the results for Samples A through E, increased levels of hydrolysis results in more compliant networks. This lower stiffness is not necessarily bad for design purposes, since it is also accompanied by an increase in damping properties, as discussed in the next section. While hydrolysis provides active sites for GA polymerization, these sites can also be saturated by adding excessive GA. Sample A+ had the same amount of hydrolysis as Sample A, but more GA, and the mechanical properties of the two samples were almost identical, which indicates that excess GA was not able to bond with the aramid nanostructures to further increase the network stiffness and strength. If the hydrolyzed sites are not saturated by GA, as for Sample C, the network is stiffened by the addition of GA (Sample B). A sample made with only PA but no GA ("No GA" sample in Figure 2a) creates hydrolyzed aramid nanostructures but cannot form the continuous network required for characterization, without either water to form hydrogen bonding or GA to form covalent bonding.

The energy absorbing capability of the materials was estimated by calculating the strain-energy density at failure, i.e., the area under the stress-strain curve, for each sample. These values that are reported in Figure 2a compare favorably with the strain-energy density of a traditional 0°/90° plain woven Kevlar mat. As shown in the Supporting Information, this mat had a strain to failure of less than 4.5%, and a strain energy density of 5.7 ± 1.4 MJ/m^3.

2.1.3. Dynamic Mechanical Analysis

The storage modulus, a measure of the elasticity, and the loss tangent, a measure of the damping or energy dissipation, were determined as a function of temperature between –100 °C and 180 °C by measuring the stress response to a dynamic strain applied at 1 Hz (Figure 2c). Above about –70 °C, the storage moduli of all the samples followed the same trend as in the tensile tests (Figure 2b), with Sample A having the highest storage modulus and Sample E the lowest. Below this temperature, the untreated specimen had the lowest storage modulus and except for the most severely hydrolyzed specimen (Sample E), all treated specimens had storage moduli exceeding that of the untreated specimen at these low temperatures. The transition at –70 °C is likely the critical temperature below which sliding motion between the smaller molecules from hydrolysis were frozen.[18–20] Many of the materials produced a pronounced peak in the loss tangent between –70 °C and –50 °C (Figure 2c2), indicating a molecular transition and increased energy dissipation, which is useful for applications requiring damping such as blast loading. This loss tangent peak decreased from Sample E to the untreated specimen, with the largest peak corresponding to the specimen subjected to the greatest extent of hydrolysis (2.5 mL PA) and lower extent of GA treatment (3.0 mL of GA in Sample E vs 3.5 mL of GA in Sample D). The drop in the peak of the loss tangent from Sample E to the untreated sample is consistent with the reduced hydrolysis and increased GA polymerization for a given amount of PA hydrolysis; both conditions that are consistent with a higher incidence of stiff, strong aramid backbone molecules.

2.2. Reaction Mechanisms of PA and GA

The nature of the functional groups created during the formation of the nanostructured networks by the PA/GA reaction was

explored using various characterization techniques. This information was used to understand how the network properties might be tailored, and to develop a general strategy to modify the networks as a polymer matrix with different characteristics for use in nanocomposites. The chemical reactions with the PA and GA were first deduced by electron-pushing diagrams. FTIR was then used to verify the proposed changes by investigating the chemical structures of the network and of the liquid product left after vacuum filtration. The different network morphologies associated with different PA/GA treatments were observed using TEM. Finally, the thermal properties of the networks were characterized by TGA to provide additional insight into the treatment effects.

2.2.1. Proposed PA and GA Chemical Reactions

As aramid macromolecules are universally known for being inert, a mechanism was required to chemically modify them and allow them to react. Hydrolysis was chosen as a method to induce reactivity by the formation of amines and carboxylic acids. **Figure 3**a describes the hydrolysis reaction of aramid molecules in a Kevlar/KOH/DMSO solution. Hydrolysis involves the splitting of a chemical bond by the insertion of a water molecule. In the case of our work, an aramid-backbone amide N–C=O bond was split to create a primary amine ($–NH_2$) and a carboxylic acid (–COOH), as shown in the reaction mechanism (Figure 3a), to allow for the subsequent condensation reaction with GA. The basic nature of the Kevlar/KOH/DMSO solution required a small amount of PA to first neutralize the base, which was a negligible amount, as just by a drop of acid, the solution changed color from red to yellow instantly and stayed yellow with more acid added. However, a stoichiometric excess of acid would be needed to have the forward reaction proceed at a higher rate than the reverse one, and the hydrolyzed products are more stable in an acidic environment. Also, given that the hydrolysis reaction requires water, a small amount (5 mL) of water was added with PA to each sample. Initially, upon addition of acid and water to the Kevlar/KOH/DMSO solution, some precipitates were observed to form owing to protonation of ANFs by water, as discussed in the companion paper.[17] However, as the reaction proceeded, the initial precipitates dissolved back into the DMSO owing to the increased polarity and smaller size of the hydrolyzed aramid chains. More detail on the role of potassium hydroxide in this process is provided in Supporting Information.

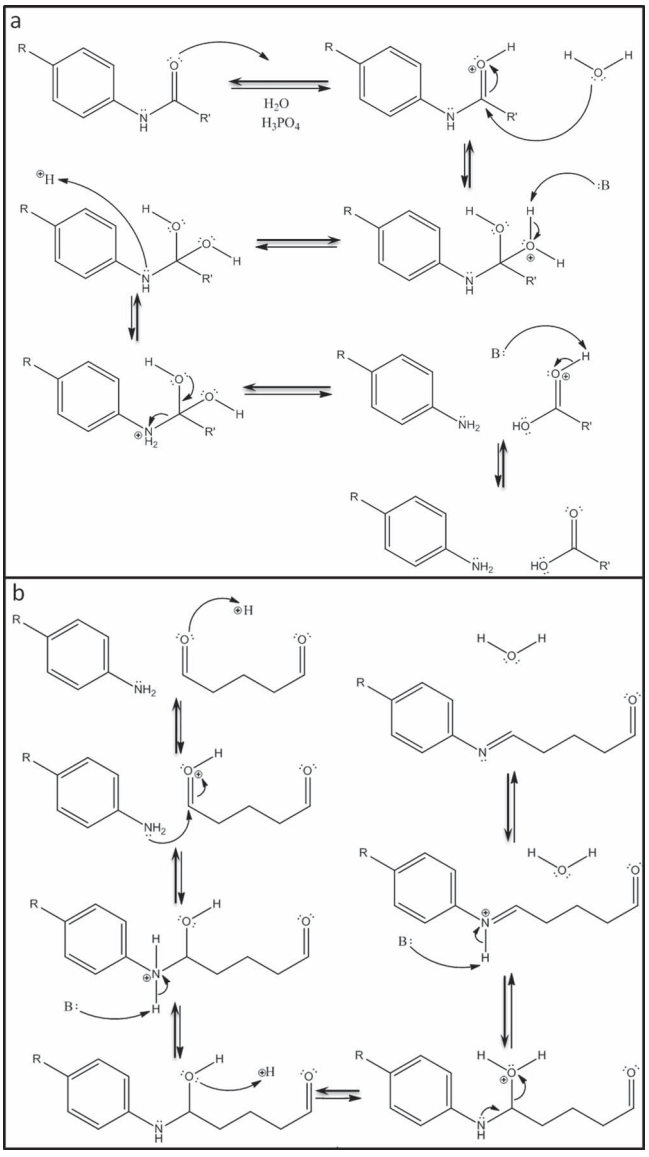

Figure 3. The proposed PA/GA reaction mechanisms with aramid molecules: a) The acid-catalyzed hydrolysis of an aramid molecule using phosphoric acid; b) Condensation of a hydrolyzed aramid molecule with GA to produce di-imines. R and R′ = aramid chain. B = any generic base.

Understanding the chemical process mechanism was of great interest to us to help in the development of a general strategy for modification and integration with other moieties to optimize stress transfer. The reactivity of the reaction products in Figure 3a, a primary amine and a benzene-conjugated carboxylic acid per amide of the original aramid backbone molecule, is high. This is convenient for creating different types of covalent bonding to polymeric and inorganic components in nanocomposites. These two functional groups can then be reacted with crosslinking agents to connect the hydrolyzed aramid backbone molecules and to manipulate the polymer properties by adding new structures to the material: a synthetic strategy that, to our knowledge, has not been previously accomplished for aramids. In this work, we considered the specific example of GA as the crosslinking agent, although a di-aldehyde or di-ketone could be used to serve the same purpose. The GA that was added to the hydrolyzed solution was 50 wt% aqueous. Given that we only used a maximum of 3.5 mL of GA solution for 100 mL Kevlar/KOH/DMSO in any sample, very little water was added and thus its effect should be small. Furthermore, by the point GA was added, the aramid molecules should have already been hydrolyzed, making further hydrolysis less likely, especially as the GA condensation worked as a competing reaction. Figure 3b shows the reactive process responsible for the polymerization owing to the formation of di-imines as the primary amines from the hydrolytic product react with GA.[21] The reaction was heated to evaporate water to promote the forward reaction.

The polymerization is complete as both aldehydes from each GA molecule undergo the reaction portrayed in Figure 3b and attach to an amine, joining two previously hydrolyzed aramid backbone molecules. GA was selected owing to its high reactivity and favorable structure, which provides two aldehydes to join two hydrolyzed aramid molecules.

2.2.2. Verification of PA and GA Chemical Reactions by FTIR

In order to verify the reaction mechanisms discussed above, FTIR was used to investigate both the solid and liquid products obtained after the vacuum filtration. The spectra performed on the networks showed clear changes associated with the PA/GA treatment when compared with the network that had no treatment, indicating that a reactive process had taken place. The results were in agreement with the mechanistic expectations discussed above, and confirmed the reactivity of the activated aramid nanostructures as convenient building blocks for nanocomposites.

FTIR spectroscopy of un-treated network shows the stretching frequency (3300 cm^{-1}, peak 1 in **Figure 4**a1) of nitrogen-hydrogen bonds and the carboxyl groups (1650 cm^{-1}, peak 2 in Figure 4a1) in amides. Peaks 3 and 4 represent respectively the bending frequencies of the amides and the aromatic carbon-hydrogen bonds in the benzene rings.[17,22,23] The aramid chemical structure is shown schematically in Figure 4a2.

FTIR spectroscopy of the networks formed after PA/GA treatment (Figure 4b1) was performed on Samples A to E following the chemical modification. The spectra showed splitting and broadening of the N–H and C=O stretches (peaks 1 and 2 in Figure 4a1), and the appearance of a new alkyl peak in GA (peak 2 in Figure 4b1). These verified that PA hydrolysis and GA condensation reactions occurred as proposed. The formation of many peaks around 3500 cm^{-1} (peak 1 in Figure 4b1) can be rationalized by the presence of different oxygen-hydrogen and nitrogen-hydrogen bonds, such as those present in imines from a condensation reaction (Figure 3b) and carboxylic acids from a hydrolysis reaction (Figure 3a). The appearance of a broad peak around 2666 cm^{-1} (peak 2 in Figure 4b1) is indicative of the presence of saturated alkyl chains from GA. The broadening and splitting of the signals around the carbonyl region (1700–1550 cm^{-1}, peaks 3 and 4 in Figure 4b1) is a result of the presence of groups such as aldehydes, carboxylic acids and imines. Different extents of reaction, caused by adding different amount of PA and GA, yielded the same spectra, although variations in the peak absorbance and intensity could be observed in each sample. The relatively low wavenumbers of amide carboxyl stretching in the range 1700–1550 cm^{-1} can be rationalized partly by the expected high degree of conjugation due to the polymer structures: Carboxyl groups usually exhibit peaks in the range of 1850–1700 cm^{-1}, but as amides are naturally conjugated with relatively low frequencies, and as they were located next to aromatic rings in the aramid backbone molecules, there was increased electronic de-localization of the group that reduced the overall wavenumber of amide carboxyl stretching (peaks 3 in Figure 4b1).[24]

From differences in the FTIR spectra between the specimens with and without treatment (Figure 4a1 and b1), especially the bands at ≈3500 cm^{-1} (peak 1 in Figure 4b1) for nitrogen-hydrogen bonds and at ≈1700–1550 cm^{-1} (peak 3 in Figure 4b1) for carboxylic acid, as well as the apparently high degree of peak overlap, it is clear that the solid product shares structural characteristics with aramids and the new alkyl group (peak 2 in Figure 4b1) that formed in the reactive processes. Different levels of PA/GA treatment resulted in different degrees of the chemical-structural changes in the networks. The proposed structure (as in Sample A) after PA/GA treatment, using limited amounts of PA, is shown in Figure 4b2. Specimens (such as Sample D) subjected to an extensive PA hydrolysis and a full GA condensation reaction process would have the structure shown in Figure 4b3, where a large number of the aramid backbone molecules, including those in the surface and core regions of the nanofibers, have been hydrolyzed and substituted with C–C bonds. This difference in the level of structural changes of the solid products, i.e., Figure 4b2,b3, was difficult to discover via FTIR. Two distinct spectra, as shown in the Supporting Information, however, were observed for the liquid residues of the reactive processes after the solid parts had

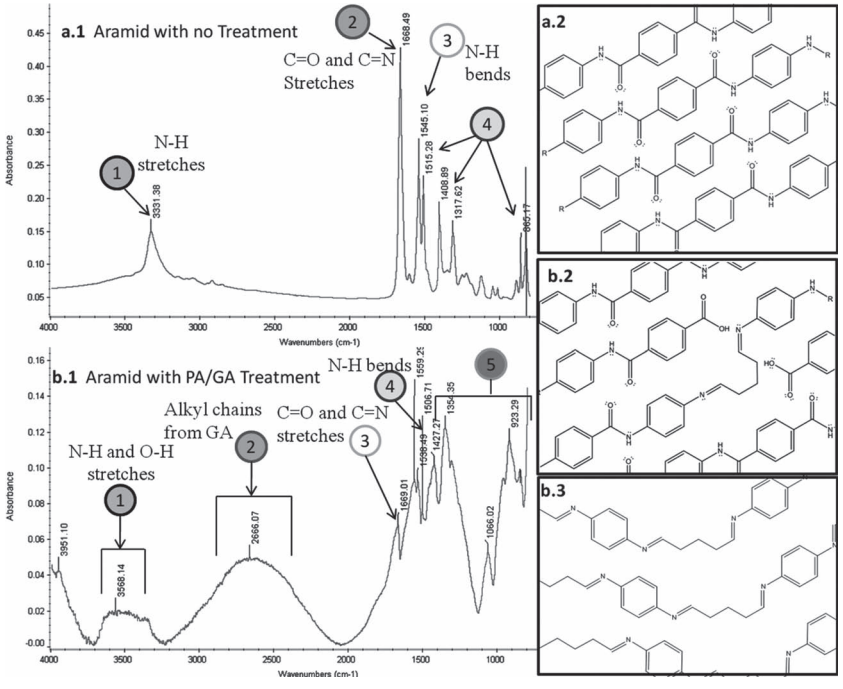

Figure 4. FTIR spectrum (a.1) of an ANF network (No Treatment), showing peaks at (1) 3331 cm^{-1}, (2) 1668 cm^{-1}, (3) 1545 cm^{-1} and (4) the fingerprint region with its corresponding structure (a.2). FTIR spectrum (b.1) of the synthetic products, nanostructured networks after PA/GA treatment (Samples A to E), showing peaks at (1) 3568 cm^{-1}, (2) 2666 cm^{-1}, (3) 1669 cm^{-1}, (4) 1559 cm^{-1}, and (5) the fingerprint region and its corresponding structure (b.2) and (b.3). (b.2): Structure of an incompletely PA hydrolyzed network, as in Sample A. (b.3): Structure of fully hydrolyzed aramid backbone molecules subjected to a full condensation process with GA (Similar to Sample D).

been filtered. They showed that reducing the amount of PA/GA reagents led to decreased hydrolysis, with correspondingly fewer carboxylic acids, i.e., the reaction product from hydrolyzation that cannot be polymerized by GA remained in the liquid residues, as well as decreased GA polymerization, with larger amounts of the unreacted GA in the solution owing to fewer functional groups formed by hydrolysis for GA bonding. The FTIR analysis of the liquid residues also agreed well with the reaction mechanisms shown in Figure 3.

2.2.3. Effect of the PA/GA Treatment on the Aramid Building Block Morphology

The effect of the PA/GA treatments on the formation of the networks was visualized using TEM to observe the morphology of the solid product left behind after evaporation from a TEM grid (**Figure 5**). Figure 5a shows the carbon-coated copper grid, and provides a reference for the subsequent images. Without any chemical treatment, the morphology in Figure 5b consists of a randomly orientated network of nanofibers; the corresponding FTIR spectrum and chemical structure are shown in Figure 4a1,a2. The morphologies of Samples A and B after each treatment step are shown in Figure 5c–f. Figure 5c shows that the nanofibers welled in the presence of a limited amount of PA (i.e., 0.25 mL of 85 wt% PA for 100 mg Kevlar). After PA-treatment, the hydrolyzed aramid molecules on nanofibers were polymerized by adding 1.5 mL of 50 wt% GA. This resulted in the morphology shown in Figure 5d, with the corresponding chemical structure and FTIR spectrum shown in Figures 4 (b1 and b2). Figure 5e shows that when a larger amount of PA was used, as in Samples B and C (e.g., 1 mL PA added to 100 mg Kevlar), nanosheets rather than nanofibers were formed after evaporation. These nanosheets were formed because the length of the nanofibers was reduced by extensive hydrolysis that broke down their aramid backbones. However, the addition of 1.5 mL 50 wt% GA to the solution resulted the restoration of a continuous network (Figure 5f), as in Sample B, owing to the condensation reaction with GA which links the aramid building blocks and forms a network, as proposed in Figure 3b. This process produced a chemical structure close to the one shown in Figure 4b3.

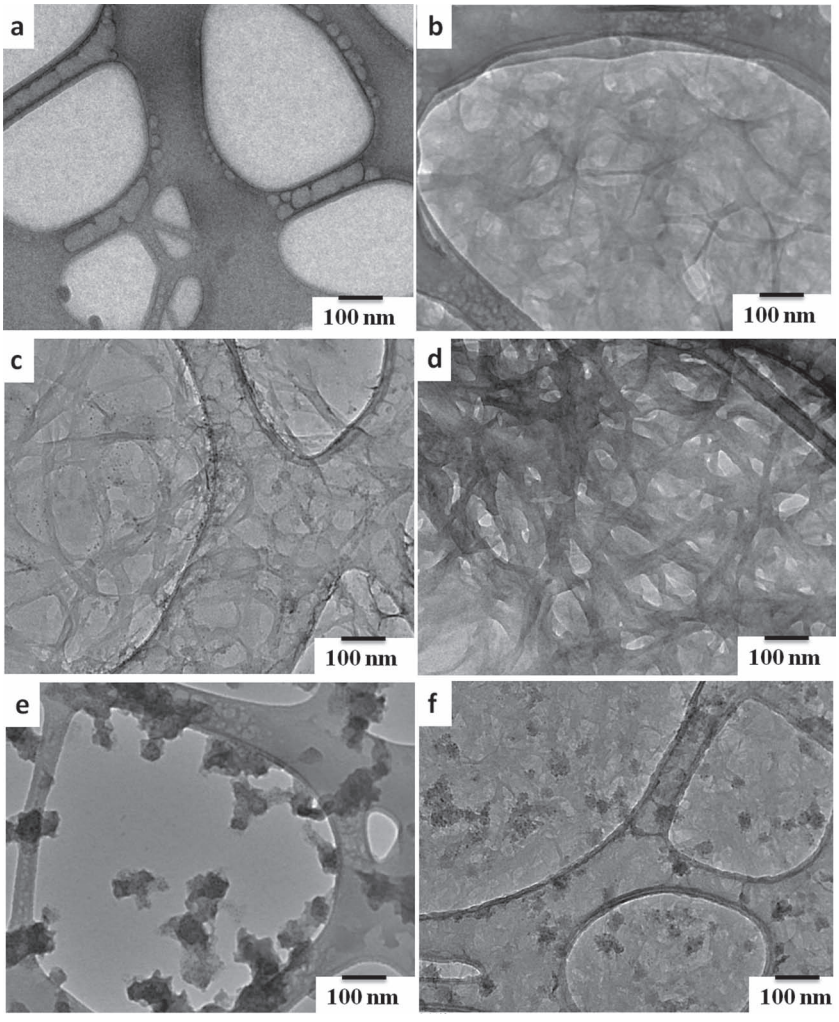

Figure 5. TEM images showing a) a carbon-coated copper grid used as the support for the TEM characterization of the networks, and the solid left after evaporation of the aramids dispersed in a DMSO solution b) with no treatment; c) after treatment of 0.25 mL PA for 100 mg Kevlar (as in Sample A but without GA treatment); d) after a further treatment with 1.5 mL GA (as in Sample A); e) after treatment of 1.0 mL PA for 100 mg Kevlar (as in Samples B and C but without GA treatment): PA-catalyzed hydrolysis turning nanofibers into reactive nanometer-scale sheets; f) restored aramid network from nanosheets in (e) after a further treatment of 1.5 mL GA (as in Sample B).

This variation in morphology provides insight into the different mechanical properties of the PA/GA treated samples. The samples prepared with less PA (Samples A through C) and, hence, with less hydrolysis (i.e., with more of the stiff aramid backbone molecules preserved), were stiffer than those that underwent more hydrolysis (Samples D and E). For the same extent of hydrolysis, the samples prepared with more GA (B and D), that underwent more polymerization of hydrolyzed chains, were stiffer than their counterparts (C and E). When the hydrolysis extent was low and GA content was high (e.g., Sample A), the GA polymerization served a crosslinking purpose to enhance the interactions between the ANFs. Although GA only has two functional groups per molecule, since hydrogen bonding keeps the rest of the hydrolyzed molecules attached to the core of the nanofiber, the polymerization between the hydrolyzed molecules from two different ANFs can be treated as a crosslinker. The ideal mechanism for obtaining a higher stiffness or strength of a network would be to limit the extent of hydrolysis to the surfaces of the nanofibers to generate reactive functional groups for GA polymerization, but without reducing the stiffness of the nanofibers. Moreover, a crosslinking agent with more than two functional groups will be more effective

than GA as it can crosslink hydrolyzed molecules from multiple ANFs together. The interactions between the nanofibers would be partially covalent with these treatment processes, compared with only secondary bonding between the nanofibers in the sample that undergoes no treatment.

With this PA/GA treatment, Sample A is essentially the optimal condition for a high stiffness and yield strength, since the network consisted of all ANFs without nanosheets, and the amount of GA used was an excess (based on Sample A+), ensuring that the hydrolyzed sites on the ANFs were polymerized to the maximum extent. That Sample A is optimal in terms of stiffness and yield strength is also supported by the fact that its response is similar to that of an 1,2-dichloroethene (DCE)-crosslinked ANF network, prepared by reacting DCE with ANFs in the Kevlar/KOH/DMSO solution at room temperature and consolidated by vacuum-assisted filtration. DCE is a crosslinker with a similar molecular structure to GA and it can crosslink aramid molecules without hydrolysis, as further discussed in Supporting Information. Thus a DCE-crosslinked ANF network should be similar to the upper bound on the stiffness and yield strength that PA/GA treated samples can reach. DCE was not the focus in this work since it does not offer as much tailorability of the sample properties as PA/GA treatment does.

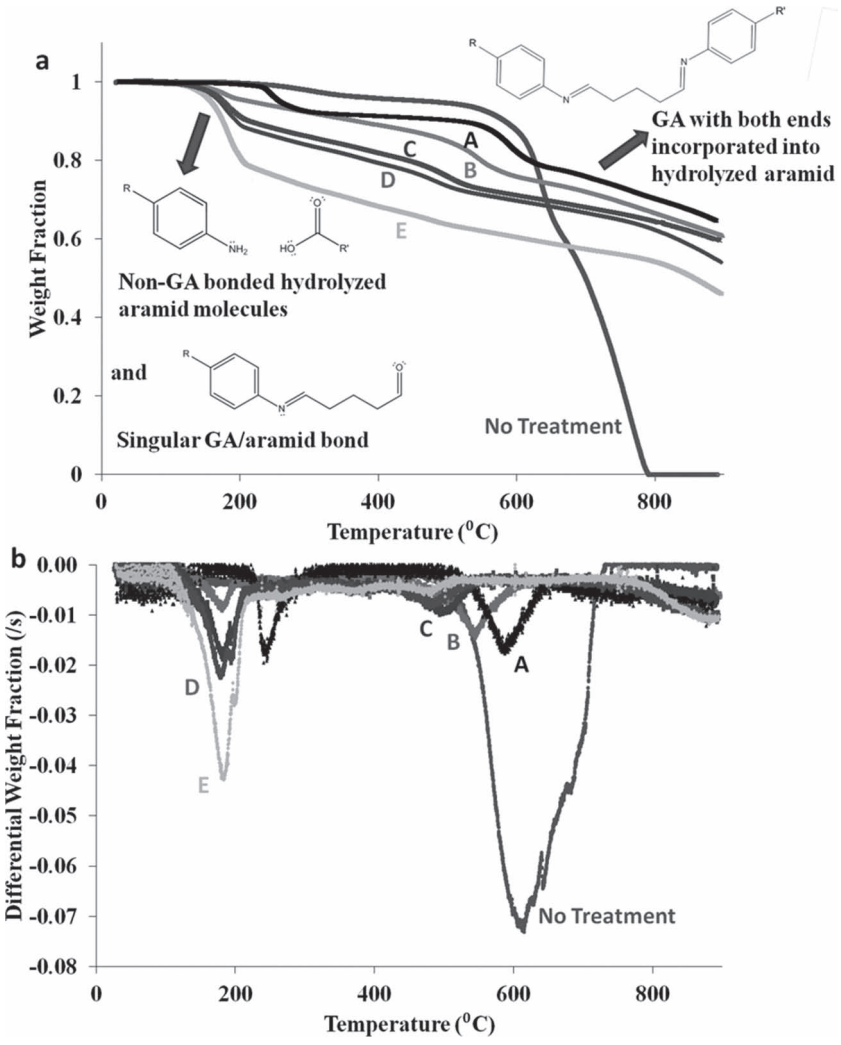

Figure 6. Characterization of the network thermal properties. a) Thermogravimetric response in air of the networks (with and without PA/GA treatment) at a temperature rise of 10 °C/min. The decomposition at ≈150 °C was proposed to be smaller aramid nanostructures created by hydrolysis but without GA polymerization. The higher thermal stability at high temperatures of the treated networks came from complete GA polymerization reactions, which improved the interactions between the aramid nanostructures in the networks. b) Rate of weight fraction decrease vs. temperature from the same TGA tests in (a). In the treated samples, more PA combined with less GA resulted in faster decomposition at ≈150 °C and slower decomposition at ≈560 °C. These results support the proposed reaction mechanisms and their effects on the network structures and properties.

2.3. Thermal Properties of Aramid Nanostructured Networks

TGA yielded two characteristic decomposition phenomena associated with the changes in the aramid nanostructured networks caused by PA hydrolysis and GA condensation. As indicated in **Figure 6**a, between 5 and 20 wt% of the PA/GA-treated samples decomposed at ≈150 °C. This decomposition came from the easily combustible aramid molecules with amide and carboxylic acid termination that resulted from hydrolysis (Figure 3a), or from the dangling aliphatic chains that resulted from incomplete GA condensation (Figure 3b). These were the smaller molecules introduced by the treatment, which resulted in a decrease of the network stiffness and strength but an increase in the damping. On the other hand, the PA/GA-treated networks showed significant improvements in high-temperature stability over the untreated one; for example, approximately 65 wt% of Sample A remained at the end of a temperature ramp test from 25 to 900 °C, while the sample with no treatment decomposed completely at ≈800 °C with the same sample weight, heating rate and air purge rate. The high-temperature stability of the PA/GA-treated samples is anomalous. It may come from aliphatic chains of GA with both ends connected to aramid backbone molecules (Figure 4b2,b3), i.e., from a complete GA polymerization process. The treated networks were harder to decompose possibly owing to a stronger interaction between the aramid building blocks. These two decomposition phenomena are also supported by the differential weight fraction plots in Figure 6b. Faster decreases in weight fraction at ≈150 °C and slower decreases at ≈560 °C were observed in the samples with more PA and less GA. This corresponds to an increase in the decomposition of the small PA-hydrolyzed molecules at ≈150 °C and a decrease in the decomposition of GA-polymerized aramid backbone molecules at ≈560 °C.

The thermal stability of the treated networks followed the same trend of their mechanical properties. It was observed that Samples D and E had decreased thermal stability compared to Samples A through C. It is conjectured that this was the result of a higher degree of hydrolysis in Sample D and E, which resulted in a higher content of easily decomposable amide and carboxylic acid terminated aramid molecules with smaller molecular sizes that decomposed at ≈150 °C (Figure 3 and Figure 5e). The sample with no treatment had no hydrolyzation and thus had no apparent drop at ≈150 °C. In addition, given the same amount of hydrolysis, Samples B and D had higher thermal stability than Samples C and E respectively, owing to a higher extent of GA polymerization in each pair, as complete GA polymerization promotes interaction between the nanostructures which was assumed to enhance thermal stability.

Given the reaction mechanisms that occur, this PA/GA treatment method should also be effective for larger-scale aramid systems, and could be potentially used to increase the interactions between Kevlar microfibers or yarns and other materials, perhaps as a solution to the previous efforts for Kevlar fibers.[6–8,10–13] However, based on previous success at the nanometer-scale,[25,26] the control over the aramid nanometer-scale building blocks, through tailoring interfacial bonding of aramid nanostructures with a high surface to volume ratio, can be used to achieve even a higher goal of making superior nanocomposites, as one approach to make nanocomposites may start with a well-tailored nanostructured matrix with good properties. The PA/GA reaction mechanisms with aramids and the tailorability of the resultant nanostructured networks shown in this work provide possibilities for the subsequent design of a nanostructured polymer nanocomposite with excellent mechanical properties to resist extreme loading. In our on-going work, we have been incorporating inorganic materials as reinforcement phases, and have achieved good interfacial bonding with the matrices with treatment, indicating promises for prospective applications of the modified aramid nanomaterials in composites.

3. Conclusions

In this work, we functionalized Kevlar with PA/GA treatment to make reactive, nanometer-scale aramid building blocks of different morphologies, which were assembled into transversely isotropic films with controlled macroscopic properties. PA was used to hydrolyze high-aspect-ratio ANFs dispersed in a DMSO solution, and to make them chemically reactive. The acid-catalyzed hydrolysis produced functional groups available for surface bonding after breaking up some of the aramid backbone molecules. These hydrolyzed aramid nanostructures were then re-polymerized by a condensation reaction with GA. The PA-hydrolysis and GA-condensation steps were used to control the properties of the resultant networks by varying the extent of the reaction at each step. When a finite but limited amount of hydrolysis and a sufficient GA condensation were applied, we obtained aramid nanostructured networks with higher stiffness, yield strength and thermal stability than those of the ANF network with no treatment. Over-hydrolysis without GA condensation rendered ANFs into discrete nanosheets, which, after being re-polymerized by GA, yielded higher network damping for energy dissipation owing to sliding between the smaller molecules, but reduced the network stiffness and strength. Moreover, the transversely isotropic properties of the aramid nanostructured films extended the anisotropy of Kevlar microfiber, with its attractive properties only along one dimension, to a planar structure, which expanded its previous use as a reinforcement phase to a matrix structure. Understanding the important effects of the PA/GA treatment and how it affects the resultant nanostructures, network morphologies and macroscopic properties, is expected to provide a basis for future work on the optimization of high-performance aramid-based structures for advanced composites.

4. Experimental Section

Synthesis: A dispersion of aramid nanofibers was achieved by reacting Kevlar with potassium hydroxide (KOH) in a dimethyl sulfoxide (DMSO) solution. Kevlar yarns (1.5 g, Figure 1d, Thread Exchange Inc., size 69, right twist) were soaked in 1-methyl-2-pyrrolidinone (NMP) (anhydrous, 99.5%, Sigma-Aldrich) and sonicated for two days to swell the fibers within the yarns and to promote the subsequent dissolution in an organic solvent such as DMSO.[27] After sonication the Kevlar fibers were washed in deionized water, thoroughly dried, and mixed with KOH (1.5 g, 99.9% semiconductor grade, Sigma-Aldrich) in DMSO (0.5 L, anhydrous, 99.9%, Sigma-Aldrich). This induced a deprotonation reaction of Kevlar by KOH.[28] The Kevlar/KOH/DMSO mixture was stirred vigorously at room temperature for seven to nine days while the solution viscosity increased and its color changed from transparent and colorless to translucent and dark red. A similar process reported in a companion paper by our group[17] results in a suspension of ANFs with diameters of 3 to 30 nm and lengths on the order of 10 μm (Figure 1b and Figure 5b).

Preparation of PA/GA-Treated Aramid Nanostructured Networks: The acidic hydrolysis of ANFs was achieved by mixing the Kevlar/KOH/DMSO solution with PA (85 wt% in water, Sigma Aldrich) and deionized water (5 mL) to promote hydrolysis. The amount of acid was varied to control the extent of reaction and is listed in Figure 2a. The mixture was heated to 373 K and vigorously stirred for 5 h. The temperature was carefully monitored and held below 383 K, the temperature at which DMSO may combust, but above 363 K, to induce hydrolysis of the amides on the aramid backbone molecules. The color of the hydrolyzed Kevlar solution depended upon the amount of acid; in general it was a clear, light-yellow liquid.

Upon completion of the hydrolysis reaction, GA (50% in water, Fisher BioReagents) was added to the hydrolyzed Kevlar/KOH/DMSO solution as a crosslinking agent after the hydrolysis reaction was complete. The amount of GA used was varied to alter the extent of reaction as listed in Figure 2a. The mixture was stirred at 373 K for three to four days. Condensation progression was monitored from the color of the mixture, which darkened and became cloudier with increased processing. The process was assumed to be complete when the color stabilized.

The resulting suspension was filtered using a hydraulic-powered pressure differential connected to a filtration flask. After pouring the products onto filter paper in a Buchner funnel, which was secured by a rubber bung on the top of the flask, a constant flow of water was used to create a pressure differential in the flask for 10–15 min until all the liquid was filtered through the paper. The color of the resulting film on the filter paper ranged from yellow to brown, depending on the extent of the reaction. A transparent-brown solution was recovered from the filtered solvent. Both the solid and liquid products were kept for subsequent analysis.

To remove any residually absorbed solvent, the recovered solid on the filter paper was placed in a 338 K oven for 24 h. After this drying process, a homogeneous film resulted, that could easily be separated from the filter paper using a razor blade.

As a comparison to the samples with the PA/GA treatment, an ANF network with no treatment was prepared by slowly adding water droplets in the Kevlar/KOH/DMSO solution at room temperature while stirring, until precipitation of protonated nanofibers was forced due to the donation of hydrogen by water.[17] The precipitation was filtered, dried and separated from the filter paper the same way as discussed above.

Characterization: The mechanical properties of the filtered films were characterized by uniaxial tensile tests. Test specimens were 1.5 mm wide and 8 to 10 mm long in the gauge section. To verify the isotropy of the samples, test specimens were cut at various in-plane orientations (plane *X*–*Y* in Figure 2a) from each sample. Each specimen was tested using an RSA 3 dynamic mechanical analyzer (DMA) (TA instruments) under a constant strain rate of 0.005 s^{-1} to ensure quasi-static loading until it fractured. The load was measured by a load cell with a maximum capacity of 3.5 N and a resolution of 1 μN. Digital image correlation (DIC) with a Grasshopper camera (Point Grey research) was used to measure displacements accurately, and the nominal strain field was computed by MetaMorph microscopy automation and image analysis software (Molecular Devices). Temperature sweep tests using the DMA were conducted from –100 to 180 °C with 10 °C min^{-1} increments at 1 Hz. A strain of 0.25 ± 0.10% was applied, from which the storage modulus and the loss tangent (tanδ) of the samples were characterized over the temperature range. The tensile and dynamic mechanical analysis data were used to determine the stress-strain responses and storage modulus and loss tangent vs. temperature responses. The thickness of the films was determined by scanning electron microscopy (FEI Quanta 3D SEM/FIB and Philips XL30ESEM). The nominal stress was determined from load data divided by the initial cross-sectional area. The Young's modulus was determined from the slope of the initial linear region of the stress-strain response curves. The yield strength was determined as the proportional limit of the initial linear region of the stress-strain response curves, up to which, stress is proportional to strain. The storage modulus and loss tangent as a function of temperature were computed by Orchestrator software (TA instruments).

FTIR spectroscopy, through a liquid-nitrogen-cooled Thermo Nicolet 6700 spectrometer (Thermo Electron Corporation), was used to probe the chemical structures of the solid and liquid products obtained from specimens with and without the PA/GA treatment in 85° grazing angle mode with a 16-mm aperture. For the liquid products, droplets of the solution were placed on top of a 10-cm diameter gold-silica wafer, covering the entire surface. In order to eliminate the additional FTIR peaks from excess solvent in the liquid products, the wafer was placed in a 338 K oven prior to FTIR inspection until the solvent evaporated entirely. At least 128 scans were taken per sample.

The morphologies of various aramids in DMSO solutions before and after the PA/GA treatments were obtained using a JEOL 3011 high-resolution electron microscope at 300 kV. One drop of solution was placed on the surface of a holey copper grid coated with carbon (Ted Pella) and the solvent was evaporated prior to TEM characterization. The aramid structures were imaged at 10 000 to 20 000 × magnifications.

The thermal properties of the PA/GA-treated aramid nanostructured networks were characterized by a thermo-gravimetric analyzer Pyris 1 (PerkinElmer) using a heating rate of 10 °C min^{-1} from 30 to 900 °C and an air purge at a flow rate of 20 mL min^{-1}. The mass of the samples was controlled between 1.35 and 1.50 mg for all tests.

Supporting Information

Supporting Information is available from the Wiley Online Library or from the author.

Acknowledgements

The authors wish to express their gratitude to Mr. Lee Mastroianni and ONR for financial support of this research (Grant No. N000141010415), Prof. Joerg Lahann for access to the FTIR machine, and Prof Ralph T. Yang and his student Nicholas R. Stuckert for access to the filtration systems and ovens.

Received: August 28, 2012
Revised: September 21, 2012
Published online: November 20, 2012

[1] X. Zhao, Q. Zhang, D. Chen, P. Lu, *Macromolecules* **2010**, *43*, 2357–2363.
[2] M. A. Rafiee, J. Rafiee, Z. Wang, H. Song, Z. Yu, N. Koratkar, *ACS Nano* **2009**, *3*, 3884–3890.
[3] J. A. Kim, D. G. Seong, T. J. Kang, J. R. Youn, *Carbon* **2006**, *44*, 1898–1905.
[4] H. C. Kuan, C. M. Ma, W. P. Chang, S. M. Yuen, H. H. Wu, T. M. Lee, *Compos. Sci. Technol.* **2005**, *65*, 1703–1710.
[5] M. Cheng, W. Chen, T. Weerasooriya, *J. Eng. Mater. Technol.* **2005**, *127*, 197–203.
[6] T. K. Lin, S. J. Wu, J. G. Lai, S. S. Shyu, *Compos. Sci. Technol.* **2000**, *60*, 1873–1878.
[7] F. Guo, Z. Zhang, W. Liu, F. Su, H. Zhang, *Tribol. Int.* **2009**, *42*, 243–249.
[8] S. Saikrasun, T. Amornsakchai, C. Sirisinha, W. Meesiri, S. Bualek-Limcharoe, *Polymer* **1999**, *40*, 6437–6442.
[9] F. H. Gojny, J. Nastalczyk, Z. Roslaniec, K. Schulte, *Chem. Phys. Lett.* **2003**, *370*, 820–824.
[10] Z. Yu, A. Ait-Kadi, J. Brisson, *Polym. Eng. Sci.* **1991**, *31*, 1222–1227.
[11] G. Li, C. Zhang, Y. Wang, P. Li, Y. Yu, X. Jia, H. Liu, X. Yang, Z. Xue, S. Ryu, *Compos. Sci. Technol.* **2008**, *68*, 3208–3214.
[12] S. Park, M. Seo, T. Ma, D. Lee, *J. Colloid Interface Sci.* **2002**, *252*, 249–255.
[13] M. Rajabian, C. Dubois, *Polym. Compos.* **2006**, *27*, 129–137.
[14] A. Mathur, N. Netravali, *J. Mater. Sci.* **1996**, *31*, 1265–1274.
[15] W. Sweeny, *J. Polym. Sci., Part A: Polym. Chem.* **1992** *30*, 1111–1122.
[16] J. W. Downing, Jr., J. A. Newell, *J. Appl. Polym. Sci.* **2004**, *91*, 417–424.
[17] M. Yang, K. Cao, L. Sui, Y. Qi, J. Zhu, A. M. Waas, E. M. Arruda, J. Kieffer, M. D. Thouless, N. A. Kotov, *ACS Nano* **2011**, *5*, 6945–6954.
[18] G. Williams, D. C. Watts, *Trans. Faraday Soc.* **1971**, *67*, 1971–1979.
[19] C. F. Hammer, *Macromolecules* **1971**, *4*, 127–129.
[20] T. Kajiyama, K. Tanaka, A. Takahara, *Macromolecules* **1997**, *30*, 280–285.
[21] H. S. Mansur, C. M. Sadahira, A. N. Souza, A. A.P. Mansur, *Mater. Sci. Eng.* **2008**, *C28*, 539–548.
[22] L. Penn, F. Milanovich, *Polymer* **1979**, *20*, 31–36.
[23] M. C. Andrews, R. J. Young, *J. Raman Spectrosc.* **1993**, *24*, 539–544.
[24] C. P. S. Hsu, in *Handbook of Instrumental Techniques for Analytical Chemistry* (Ed: F. A. Settle) Prentice-Hall, NJ, USA **1997**, p. 254.
[25] P. Podsiadlo, A. K. Kaushik, E. M. Arruda, A. M. Waas, B. S. Shim, J. Xu, H. Nandivada, B. G. Pumplin, J. Lahann, A. Ramamoorthy, N. A. Kotov, *Science* **2007**, *318*, 80–83.
[26] A. K. Kaushik, P. Podsiadlo, M. Qin, C. M. Shaw, A. M. Waas, N. A. Kotov, E. M. Arruda, *Macromolecules* **2009**, *42*, 6588–6595.
[27] I. O'Connor, H. Hayden, J. N. Coleman, Y. K. Gun'ko, *Small* **2009**, *5*, 466–469.
[28] R. R. Burch, L. E. Manring, *Macromolecules* **1991**, *24*, 1731–1735.